Transportation Geotechnics 19 (2019) 19–34

Contents lists available at ScienceDirect

Transportation Geotechnics

journal homepage: www.elsevier.com/locate/trgeo

Railroad infrastructure 4.0: Development and application of an automatic ballast support condition assessment system

Yu Qian[a,*], Marcus S. Dersch[b], Zhengboyang Gao[c], J. Riley Edwards[b]

[a] Department of Civil and Environmental Engineering, University of South Carolina, 300 Main Street, Columbia, SC 29208, USA
[b] Rail Transportation and Engineering Center – RailTEC, Department of Civil and Environmental Engineering, University of Illinois at Urbana-Champaign, 205 N. Mathews Ave., Urbana, IL 61801, USA
[c] Saiful Bouquet Structural Engineers Inc., 155 N Lake Ave. #600, Pasadena, CA 91101, USA

ARTICLE INFO

Keywords:
Industry 4.0
Automation
Cyber-physical systems
Big data
Railway track structure
Concrete sleeper
Ballast
Optimization algorithm
Laboratory experimentation
Field application
Real-time monitoring

ABSTRACT

Industry 4.0, or the fourth industrial revolution, is the current trend of automation and data exchange in manufacturing technologies. Even though Industry 4.0 emerged as a manufacturing initiative, the idea of bridging digital and physical systems can be expanded beyond the manufacturing industry. "Railroad Infrastructure 4.0" is thus proposed in this study to revolutionize the maintenance operations of the railroad industry. In North America, most primary freight and passenger rail corridors are constructed using ballasted track. One of the primary maintenance activities is to ensure the ballast is performing adequately. Being able to monitor the ballast condition and conduct tamping operations (e.g. maintenance activities) at optimal intervals can increase the safety and efficiency of railroad operations. Previously, techniques such as ground penetrating radar (GPR) and Matrix Based Tactile Surface Sensors (MBTSS) have been used to assess the condition of ballast, but these investigative tools lack the capability of automatically and continuously monitoring the track system. Researchers at the University of Illinois at Urbana-Champaign and the University of South Carolina have developed a non-intrusive method as a key component of Railroad Infrastructure 4.0 to continuously quantify ballast pressure distribution (i.e. ballast condition) under the sleeper (also known as a "crosstie"). This method innovatively uses the bending moment profile across the concrete sleeper, and the approximated rail seat loads as inputs, to back-calculate the ballast support condition through the use of an optimization algorithm. The ballast support condition assessment system that was developed has been validated for accuracy from extensive laboratory experimentation. The laboratory validated system was deployed in the field on a Class I heavy axle load (HAL) freight railroad in the United States to continuously monitor the ballast pressure distribution beneath concrete sleepers in real-time under revenue service operating conditions. The evaluation of ballast pressure distributions between adjacent sleepers as well as tonnage accumulated are also included. To better quantify the variation of ballast pressure beneath the sleepers, the Ballast Pressure Index (BPI) is also proposed. The information presented in this paper demonstrates the concept and potential of Railroad Infrastructure 4.0 as a future framework for railroad maintenance planning and management.

Introduction and background

Industry 4.0

From the first revolution of mechanization using water power and steam power, to mass production and the assembly line, to the more recent achievement of further automation of manufacturing using electronics and Information Technology (IT), the manufacturing industry has undergone significant transformation. Industry 4.0, or the original German "Industrie 4.0", represents the fourth industrial revolution [11]. By converging IT and Operational Technology (OT) with the hyper-connected digital industry, Industry 4.0 introduces what has been called the "smart factory," in which cyber-physical systems (CPS) monitor the physical processes of the factory and make decentralized decisions [11]. Not limited to manufacturing industry, the concept, principles, and technologies of Industry 4.0 are now being increasingly adopted by other industries. Amazon's automated shipment centers are large-scale examples of the CPS working toward Industry 4.0 [30]. The leading online marketplace's "fulfillment centers" already rely on more than 15,000 robots to pick out merchandise for

* Corresponding author.
E-mail addresses: yuqian@sc.edu (Y. Qian), mdersch2@illinois.edu (M.S. Dersch), zgao@saifulbouquet.com (Z. Gao), jedward2@illinois.edu (J.R. Edwards).

https://doi.org/10.1016/j.trgeo.2019.01.002
Received 19 July 2018; Received in revised form 19 November 2018; Accepted 21 January 2019
Available online 22 January 2019

orders. The company also utilizes one of the largest robotic moving arms in the world to help transfer pallets. The key to the robotic warehouse's success is that robots can learn, self-adjust, and aggregate and share data from other pods to troubleshoot issues among themselves [30].

Railroad Infrastructure 4.0

Throughout history, the railroad industry has witnessed various changes and improvements; especially in recent years, with the development of Automatic Train Control (ATC) and Automatic Train Protection (ATP) systems [28,7], as well as the anticipated launch of a driverless freight railway in Australia [25], railroad operation has entered the automation era. However, on the railroad track maintenance side, manual labor is still highly relied upon due to the fact that a sizeable portion of maintenance activities are prioritized based on results from periodic visual inspection. Without an automated and systematic monitoring system, railroad infrastructure lacks proper and cost-efficient maintenance operations. Therefore, adopting the concept of Industry 4.0 and adjusting it to the railroad industry, Railroad Infrastructure 4.0 is proposed as an integrated and automated system that would allow the railroad infrastructure to diagnose the problems among its components and maintain itself.

The proposed Railroad Infrastructure 4.0 framework consists of four key elements: Sensor Monitoring, Cloud Computing, Decision Making, and Problem Solving. As can be seen in Fig. 1(a), railroad track infrastructure consists of two parts, superstructure (rails, sleepers, and fastening system), and substructure (ballast, sub-ballast, and subgrade). A failure in either part of the infrastructure can potentially endanger the safe and efficient operations of railroads. During Sensor Monitoring, sensors installed in the superstructure and substructure of the railroad track infrastructure are automatically and constantly monitoring the behavior of the track system and its components. As highlighted in Fig. 1(b), several monitoring techniques have already been successfully implemented in the field and can be integrated into Railroad Infrastructure 4.0. The Wheel Impact Load Detector (WILD) is currently used by North American and international railways to monitor the static and dynamic wheel loads that are applied to the infrastructure [16]; the concrete surface strain gauge was first deployed in the field by researchers at UIUC to measure and analyze the in-service flexural demand of concrete sleeper [8,9]; a "SmartRock", a 3-D printed rock with built-in electronics developed by researchers at the Pennsylvania State University, has been installed on test tracks at the Transportation Technology Center (TTC) and has proven to provide valuable measurements on ballast particle movement [18]. The combination of measurements collected from these sensors can indicate the track condition at any given time. While the sensors are collecting measurements, data are simultaneously transferring to the cloud server for post-analysis. To convert raw measurements into valuable information in a timely manner, a set of cost-efficient algorithms need to be developed for Cloud Computing. Big Data analysis techniques should be implemented during this process to minimize the computation time. Several limits (e.g. maximum input load, maximum bending strength, maximum displacement) must be established at the beginning such that once a value exceeds a set limit, the Decision Making stage will be triggered and the end-users (i.e. railroad track department directors), will be alarmed. End-users will respond with a request for certain maintenance activities and they will be carried out during Problem Solving, possibly by autonomous maintenance rail vehicles in the future.

The four elements in Railroad Infrastructure 4.0 create a loop for automated and cost-efficient railroad track maintenance operations. Though human interference may be required during Decision Making and Problem Solving stages, these processes can ultimately mature to

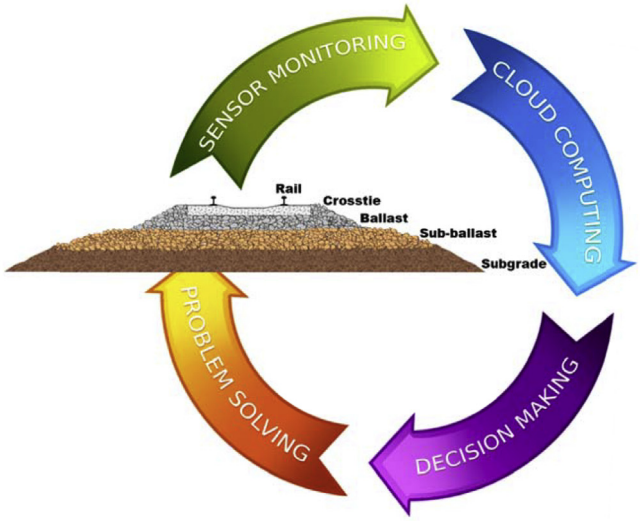

(a) Conceptual framework

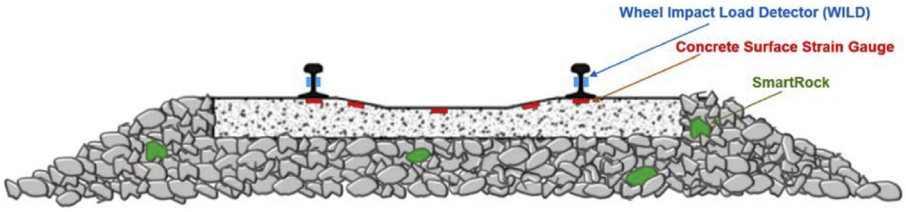

(b) Example of in-track sensors

Fig. 1. Railroad Infrastructure 4.0: (a) Conceptual framework; (b) Example of in-track sensors.

full automation. Railroad Infrastructure 4.0 is a self-learning system. It will adapt from the decisions made by end-users over numerous combinations of results analyzed during Cloud Computing and eventually be able to provide the most suitable decision by itself. With the recent development of autonomous vehicles and the fast-growing robotic techniques, maintenance activities can be conducted automatically with minimum human supervision in the near future. Also, as an Internet of Things (IoT), Railroad Infrastructure 4.0 is capable of adapting to new techniques and integrating upgrades in each of the four elements. The remainder of the paper will introduce a recently developed technique for automatically assessing the ballast condition within the railroad track infrastructure and demonstrate how it can be implemented as a useful upgrade to Railroad Infrastructure 4.0.

Development of automatic ballast support condition assessment system

Ballast material and previous research

In North America, the majority of railroad track infrastructure is supported by ballast. Ballast is usually packed between, below, and around the sleepers [26]. Beyond bearing and distributing the load from the sleepers to the substructure, ballast also facilitates the drainage of water, keeps vegetation from interfering with the track structure, and provides lateral stability and holds the track in place during the passage of trains [26]. In 2013, North American railroads added around 10.3 million cubic meters (13.5 million cubic yards) of ballast to the track structure for new construction and maintenance projects [2].

A variety of materials have been used for ballast over the years, but crushed stone, such as granite and hard sandstone, is considered to be the premium ballast material and has long been preferred for mainline applications [20]. A well-performing ballast material should be hard, angular, uniformly graded, and have a rough surface texture [24]. However, because of its granular property, repeated train loads can cause plastic ballast deformation within the ballast layer which in-turn leads to ballast breakage, track settlement, and track geometry deviations [24,17,23,13,6,27]. These ballast deterioration mechanisms rearrange the ballast distribution and change the support condition beneath the sleepers, not only increasing the risk of track geometry deviations, but also affecting the bending behavior of sleepers, as the sleeper's flexural performance is highly sensitive to its support condition [31,32].

To prevent ballast deterioration from jeopardizing safe railroad operations, several techniques have been employed to inspect and investigate the ballast condition. The traditional technique is visual observation of the track, but it is superficial and is mostly used to look for mud pumping or standing water [24]. Advanced techniques have been developed in recent years to investigate the ballast condition at the sleeper-ballast interface. A hi-rail-based or geometry-car-mounted ground penetrating radar (GPR) system can record the subsurface profile and ballast particle distribution beneath sleepers along the track [29]. However, GPR inspections typically occur at certain fixed intervals and the methodology does not facilitate continuous monitoring of ballast condition or recording data under the passage of trains. Installing a Matrix Based Tactile Surface Sensor (MBTSS) system along the bottom of the sleeper can capture the ballast pressure distribution directly beneath sleepers, but it requires jacking the rail and sleepers during installation of the sensors, thus disturbing the ballast [21]. Furthermore, the pressure sensors are fragile and high loads induced by train passes as well as environmental conditions can result in failure of the sensor within a relatively short period of time. With these challenges in mind, a non-intrusive, computer-aided technique to accurately and continuously measure the ballast condition in a timely manner is needed.

Development approach

Since maintaining the health of track ballast is of vital importance to the robustness of railroad infrastructure, certain techniques need to be incorporated into the loop of Railroad Infrastructure 4.0 to ensure an automatic and systematic approach towards monitoring and assessing the ballast condition. Knowing that it is inherently difficult to directly measure the ballast condition at the sleeper-ballast interface, researchers at UIUC and USC have developed an indirect technique, which can be readily adopted into Railroad Infrastructure 4.0, to quantify the ballast support condition beneath concrete sleepers. Based on force equilibrium and the basic principles of statics, for a two-dimensional subject, only one combination of reaction forces (one support condition) can account for a certain bending moment profile under a set of applied loads. Following this logic, if the concrete sleeper is simplified as a two-dimensional beam, then its ballast support condition can be back-calculated from the bending moments along the concrete sleeper and the corresponding rail seat loads, both of which can be quantified during either laboratory or field experimentation [8].

Concrete surface strain gauges have proven capable of capturing the bending strains experienced by concrete sleepers during previous laboratory and field experimentation [8], and are expected to be a key component within the Sensor Monitoring element of Railroad Infrastructure 4.0. The bending strains can be converted into bending moments when calibration factors, which can be determined in the laboratory, are applied. Loading configurations used for calibration tests are adapted from tests specified in Chapter 30, Section 4.9 in the American Railway Engineering and Maintenance-of-Way Association (AREMA) Manual for Railway Engineering (MRE) (2016). Fig. 2 illustrates the typical layout of strain gauges installed on a 260 cm (102 in.) long concrete sleeper. A total of five strain gauges (labeled A - E) are installed, oriented longitudinally along the chamfer, near the top surface of the sleeper. Because the sleeper is not fixed (no restraint) at two ends in any ballast support condition, the bending moments at two ends should equal to zero. Therefore, when combined with five measured moments from strain gauges, the sleeper has a total of seven known bending moments at seven discrete locations.

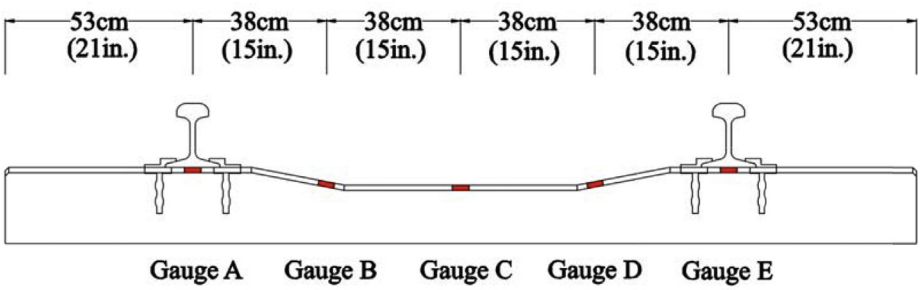

Fig. 2. Profile view of a typical instrumented concrete sleeper (red lines indicate surface strain gauge locations). (For interpretation of the references to color in this figure legend, the reader is referred to the web version of this article.)

The values of rail seat loads are obtained differently under laboratory and field experimentation. In the laboratory, rail seat loads can be monitored and recorded through either calibrated pressure gauges or calibrated load cells. In the field, rail seat loads are indirectly computed using the AREMA recommended equation (Eq. (1)) [1], from the wheel loads provided by nearby WILD sites or similar vertical rail-mounted wheel load strain gauge circuits, both of which can be incorporated into the Sensor Monitoring element of Railroad Infrastructure 4.0.

$$R = WL \times DF \times (1 + IF) \quad (1)$$

where R = design rail seat load (kN)

WL = unfactored wheel load (kN)
DF = distribution factor (from AREMA MRE Figure 30-4-1)
IF = impact factor (specified as 200% by AREMA).

AREMA assumes rail seat loads to be point loads when calculating the bending moments [1]. However, in order to consider a more realistic loading scenario, rail seat loads are assumed to be uniformly distributed across the rail seats in the ballast support condition back-calculator.

Fig. 3 shows the two-dimensional sleeper model that the back-calculation is based on. The model represents a 260 cm (102 in.) long concrete sleeper typically used in North American heavy haul freight railroad infrastructure. As mentioned above, the rail seat loads are assumed to be uniformly distributed over the 15 cm (6 in.) rail seat. The sleeper was divided into six discrete bins of equal size (numbered 1–6), so that the width of each bin was 43 cm (17 in.). Each bin will carry a certain percentage of the total ballast reaction force, and within each bin, the reaction force was also assumed to be uniformly distributed. The reaction force distribution in Fig. 3 demonstrates a scenario where the ballast support is uniform along the entire sleeper, but it is not intended to represent an actual result from the back-calculator. The strain gauge layout of the sleeper model is identical to that of the instrumented sleepers mentioned earlier. Therefore, a total of nine back-calculator inputs, consisting of seven known bending moments and two approximated rail seat loads, can be used in the sleeper model. In addition, two boundary conditions are included for computation. First, based on force equilibrium, the total ballast reaction force should equal the total rail seat loads, thus the sum of all six bins should be approximately 100%. Second, the value of each bin should not be less than zero, as it is unrealistic to have a negative reaction force for ballast.

During the development stage, the automatic ballast support condition assessment system is simulated as a standalone support condition back-calculator, with features that could be later adopted into Railroad Infrastructure 4.0 (see Section 3 for field application). The ballast support condition back-calculation process is summarized in the flowchart below (Fig. 4). First, the standalone back-calculator allows the user to define the input rail seat loads as well as the bending moments at the five strain gauge locations along the sleeper. The magnitudes of those inputs should represent a true set of laboratory experimentation results or in-field measurements. When incorporated into Railroad Infrastructure 4.0, the input rail seat loads will be automatically computed and defined based on the measurements gathered from the Sensor Monitoring element. Second, the back-calculator will generate a support condition, which consists of random combinations of reaction forces. This random support condition is disregarded if it does not meet the pre-established boundary conditions, and the computation would only proceed to the next step once both boundary conditions are satisfied. Third, from the values of rail seat input loads and the generated support condition, the back-calculator would compute a matrix of seven bending moments along the sleeper. The calculated bending moment matrix will then be compared with the matrix of the seven input bending moments. The back-calculator would go back and generate a new set of support condition if the matrix difference is found to be significant. The iteration would terminate when the difference between two matrices reached its minimum. An optimization algorithm was implemented into the iteration process to reduce the computational time. In the end, the back-calculator generated the combination of reaction forces that induced the matrix of input bending moments as the resultant support condition. The ballast reaction forces could be later converted into ballast pressures by dividing the forces over the bottom width of the sleeper. When the assessment system is eventually included into Railroad Infrastructure 4.0, the entire iteration process will be conducted within the Cloud Computing element (see Section 3 for field application).

For a certain set of input loads and reaction forces, shear force and bending moment profiles can be determined by applying the principle of statics [12]. If the variations of shear force and bending moment were considered as functions of position, x, along the length of the sleeper, the equations for calculating the change in shear force and change in bending moment could be written as shown below.

$$\Delta V = \int w(x)dx \quad (2)$$

$$\Delta M = \int V(x)dx \quad (3)$$

where ΔV = change in shear force (kN)
w(x) = intensity of the loading along the sleeper (kN/m)
V(x) = magnitude of shear force along the sleeper (kN)
ΔM = change in bending moment (kN m).

The change in shear force equals the area under the loading diagram. Since the loading condition was known, the shear force diagram could be produced along the entire length of the sleeper. The change in bending moment equals the area under the shear force diagram. Since there was no bending moment at either end of the sleeper, the entire bending moment diagram could then be developed.

In order to apply the two equations above to capture the continuous bending moment profile, the bending strain must be known at every infinitely small interval along the sleeper to seek the unique solution. Instrumentation such as laser and optical fiber can potentially achieve this goal [22,4], but in the development stage of the ballast support condition assessment system and due to the limitation of the discrete strain gauge installation, Eqs. (2) and (3) needed to be modified to calculate the bending moment at each discrete location. Fig. 5 demonstrates a sample calculation process. As mentioned earlier, a concrete sleeper can be simplified as a simply-supported two-dimensional beam (Fig. 5(a)). Vertical rail seat loads (R_1 and R_2) acted as uniformly distributed loads. Based on previously defined loading conditions,

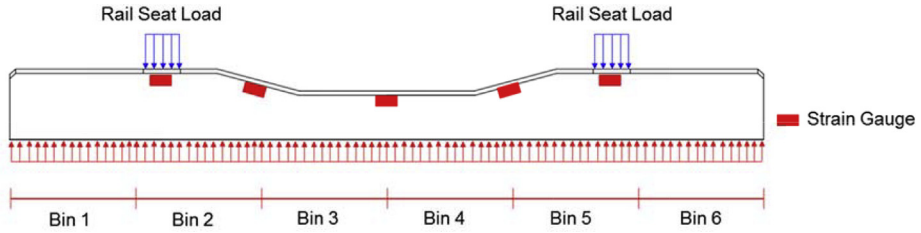

Fig. 3. Sleeper model for ballast support condition back-calculator (with assumed uniform support condition).

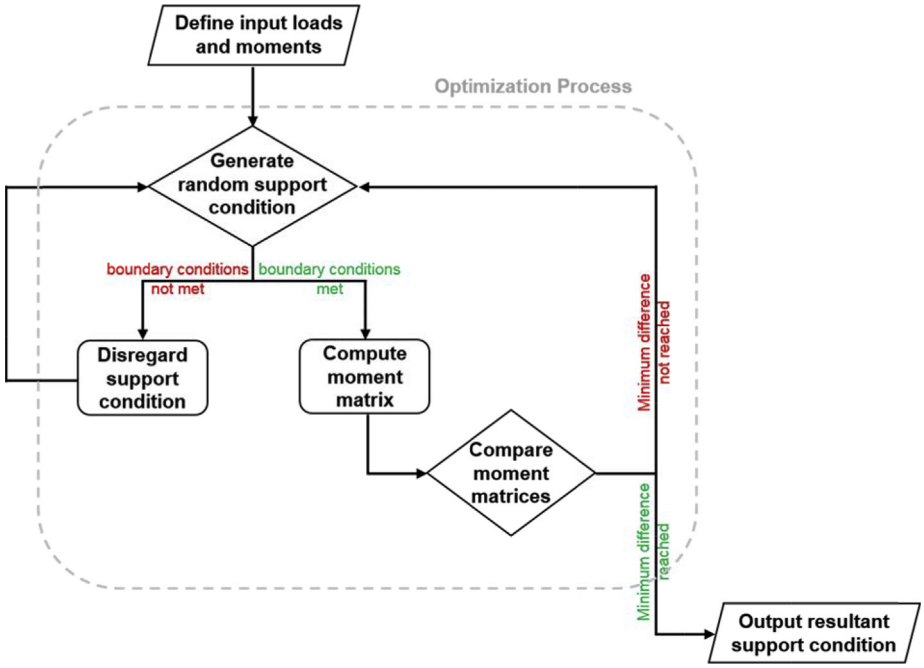

Fig. 4. Flowchart for ballast support condition assessment system.

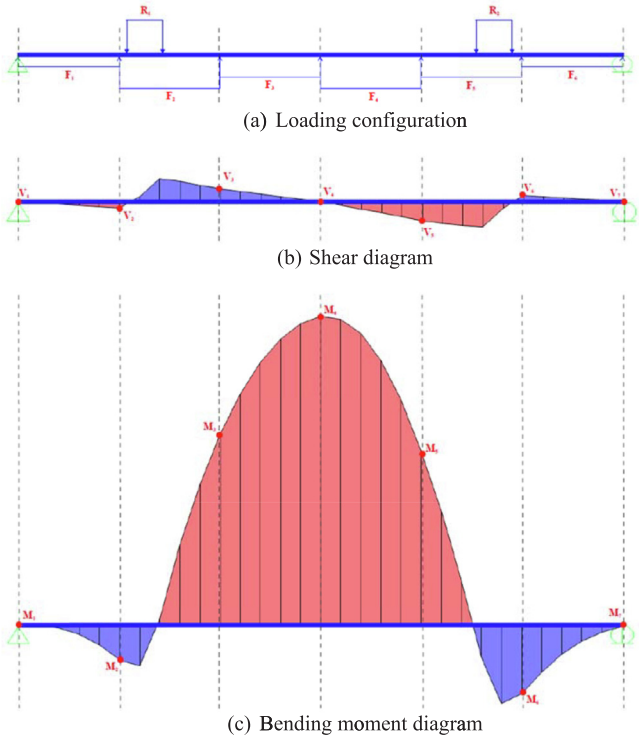

Fig. 5. Two-dimensional model sample calculation (a) Loading configuration, (b) Shear diagram, (c) Bending moment diagram.

ballast reaction forces were evenly divided into six bins and within each bin, the reaction force was uniformly distributed. As shown in Fig. 5(a), a random set of ballast reactions were applied to the beam, but the following relation needed to be achieved to satisfy the pre-established boundary condition.

$$R_1 + R_2 = \sum_{i=1}^{6} F_i \tag{4}$$

where, R_1, R_2 = rail seat load magnitude over each rail seat (kN)
F_i = total ballast reaction within each sleeper bin (kN).

Once the loading configuration was set up, the shear and bending moment diagram (Eq. (5)) could then be calculated based on Eqs. (2) and (3), as shown in Fig. 5(b) and (c). However, since the purpose of this entire process was to compare the calculated bending moments with the measured bending moments from the strain gauges, bending moments from only seven discrete locations (highlighted in Fig. 5(c)) were required, and they were calculated within the model by using the equation below.

$$M_i = \begin{cases} \sum_{j=1}^{i} F_{j-1}\frac{(1-j)l}{2} (1 \le i \le 2) \\ R_1\left[(i-4)l + \frac{g}{2}\right] - \sum_{j}^{i-1} F_j(i-j-\frac{1}{2})l (3 \le i \le 5) \\ R_1\left[(i-4)l + \frac{g}{2}\right] + R_2\left[(i-4)l - \frac{g}{2}\right] \\ \quad - \sum_{j=1}^{i-1} F_j\left(i-j-\frac{1}{2}\right)l (6 \le i \le 7) \end{cases} \tag{5}$$

where, R_1, R_2 = rail seat load magnitude over each rail seat (kN)
F_i = total ballast reaction within each sleeper bin (kN)
l = length of sleeper bin (m)
g = gauge distance (distance between centers of rails) (m).

To provide the most accurate results, the difference between measured and calculated values need to be minimized. A normalized value was thus used to determine the difference between the computed and input bending moments. The equation for calculating this normalized value is listed below (Eq. (6)). This value should always be greater than or equal to zero. As the iterations begin to converge, this value should stay relatively stable around its minimum, and for the last five iterations, the percent difference among those normalized values should be within 1%. Note, the difference between the calculated values and target values exist due to numerical iterations. With a fixed set of the input strains, because there are more knowns than unknows, the calculated ballast support condition is unique with given numbers of steps during iterations. In other words, the solution is unique.

$$norm = \sqrt{\sum_{n=1}^{7} (M_{cal,n} - M_{ipt,n})^2} \quad (6)$$

where, norm = normalized value of the difference between matrices of input moments and calculated moments and:

$M_{cal,n}$ = calculated bending moment at nth discrete location from the left end of the sleeper
$M_{ipt,n}$ = input bending moment at nth discrete location from the left end of the sleeper.

Optimization algorithm

During the development stage, MATLAB was chosen as the programming language for the optimization process. Because MATLAB uses the matrix as its basic data element and employs vectorized operations [19], it expedited the optimization process of the back-calculator as matrix-based computation was regarded as a crucial step during the iteration. Further, the user-friendly interface in MATLAB facilitated accelerated development of the algorithm and will eventually improve end-user experience. However, due to the possibility for large amounts of data flowing inside Railroad Infrastructure 4.0, the programming language is subject to change to adapt the algorithm for faster processing speed.

Bi-polar Pareto Distribution, a long-tailed probability distribution, was used as the random variable generator to generate a random combination of reaction forces during the iteration process. The equation for generating random variables is shown below as Eq. (7) [10].

$$r = \frac{s}{10^{-20}} \frac{(\alpha - 1.0)}{\left(\frac{10^{-20}}{10^{-20} + rand}\right)^{-\alpha}} \quad (7)$$

where, r = generated random variable (between 0.0 and 1.0)

s = fair coin flip (equal probability of −1.0 and 1.0)
α = excursion parameter (ranges from 1.0 to 2.0)
rand = random variable generated from uniform probability distribution (between 0.0 and 1.0).

The reason for choosing a bi-polar Pareto Distribution over a uniform probability distribution as the random variable generator was that, when compared to using random variables drawn from uniform probability distribution, random variables drawn from long-tailed probability distributions result in super-diffusive search behaviors that enable the iteration process to cover the entire dataset more quickly and thoroughly [10]. The reason for choosing bi-polar Pareto Distribution over other long-tailed probability Distributions was that Pareto Distribution could find better solutions in less time without being significantly affected by reasonable variations in the excursion parameters of the probability distributions [10].

Simulated annealing was chosen as the probabilistic technique for approximating the global optimum of the iteration process. One important characteristic of simulated annealing was that it had a probability of accepting a "worse" solution [14]. The acceptance probability function used to determine whether to obtain a solution is listed in Eq. (8).

$$ap = e^{\frac{(norm_{old} - norm_{new})}{T}} \quad (8)$$

where, ap = acceptance probability

$norm_{old}$ = normalized value of the difference between matrices of input moments and calculated moments from the previous iteration
$norm_{new}$ = normalized value of the difference between matrices of input moments and calculated moments from the current iteration
T = temperature (greater than 0.00001).

The acceptance probability (ap) was compared to a random variable (between 0.0 and 1.0) generated from uniform probability distribution after each iteration. If ap was greater than the random variable, the back-calculator would abandon the combination of reaction forces from the previous iteration and accept that from the current iteration as a better solution. If not, the back-calculator would keep the combination from the previous iteration as the better solution. As can be seen from Eq. (6), as long as the difference between input and calculated moments was larger in the previous iteration than in the current iteration, ap would be greater than 1.0, meaning that simulated annealing would always accept the result from the current iteration if it could generate a better solution. However, when the result from the current iteration generated a worse solution, it is possible that simulated annealing would allow the back-calculator to accept the worse solution. This could be beneficial when the iteration process was stuck at a local optimum. No better solution could be found near a local optimum, so temporally accepting a sub-optimal solution would help the back-calculator to "jump" out of the local optimum.

The characteristic of occasionally accepting poorer solutions is the major difference simulated annealing has as compared to the general hill climbing algorithms [15]. A typical hill climbing algorithm simply accepts neighbor solutions that are better than the current solution. The algorithm stops when it cannot find any better neighbors. However, considering all the solutions of a given optimization problem as many hills, the best solution being the highest hill. If the plan was to only climb upward, the climber would reach a point where he or she could no longer climb any higher without first descending. Similar to this analogy, simulated annealing prevented the back-calculator from getting stuck at any local optima by allowing the back-calculator to sporadically choose worse solutions over seemingly better ones.

The temperature term, variable T (which is not related to a measure of heat), was used in Eq. (6) as a scale factor to adjust the ap value. At the beginning of the iteration process, T was set to be a value greater than 0.00001, which would provide the proper amount of randomness into optimization to escape local optima early in the process, and it would gradually decrease as the iteration progressed, increasing the ap value and lowering the possibility of accepting a worse solution. As the iteration process came to an end, T would approach 0.00001, making it very unlikely to accept a worse solution and highly likely to find the global optimum. Fig. 6 shows a pseudocode that demonstrates a simplified version of the optimization algorithm. The variable β was introduced in Line 4 of the code. This variable was defined as the rate of decrease for variable T; that is, the lower the β value was, the faster the variable T reached its minimum. In Line 6, a cumulative variable, i, was introduced. This variable increased by 1 after each loop of iteration for every T value, and the total number of iterations for each T value was defined in Line 7 (200 iterations shown in the pseudocode).

The values of the variables α, T, β, and i need to be tuned to optimize the efficiency, accuracy, as well as consistency of the ballast

```
1   old_moment = back-calc(support)
2   T = 8.0
3   T_min = 0.00001
4   β = 0.99
5   while T > T_min
6       i = 1
7       while i <= 200
8           new_support = neighbor(support)
9           new_moment = back-calc(new_support)
10          ap = acceptance_probability(old_moment, new_moment, T)
11          if ap > random()
12              Support = new_support
13              old_moment = new_moment
14          i = i + 1
15      T = T * β
16  return support
```

Fig. 6. Pseudocode for the optimization algorithm.

Table 1
Results of parametric studies.

CASE	α	T	β	i
Initial	2.0	8.0	0.90	200
Part 1	1.0 ~ 2.0	8.0	0.90	200
Part 2	**1.227**	1.0 ~ 8.0	0.90	200
Part 3	**1.227**	**4.0**	0.0 ~ 0.90	200
Part 4	**1.227**	**4.0**	**0.85**	200 ~ 800
Optimal	**1.227**	**4.0**	**0.85**	**550**

support condition assessment system. Therefore, a series of parametric studies were conducted to obtain the optimal values of those variables. One particular set of bending moments and rail seat loads was imported into the back-calculator as inputs to generate resultant support conditions based on different combinations of variable values. Initially, 2.0, 8.0, 0.9, and 200 were assigned to the variables, respectively. The parametric studies were divided into four parts; for each part, one variable was tested on numerous values while the other three variables remained unchanged. For example, in Part 1, several values of α within the range of 1.0–2.0 were tested, but variables T, β, and i remained constant. For each set of variables, twenty randomized initial support conditions were used to compute the resultant support conditions. Average computational time and sum of normalized values for all twenty tests were recorded. After each part of parametric studies, an optimal value of the changing variable would be determined as it generated the results with least average computational time and the sum of normalized values.

Table 1 illustrates the process and the results of the parametric studies. For each part of the parametric studies, the cell containing the variable subject to changes was filled with green color. After each part, the optimal value of the changing variable was bolded and shown right below the color-filled cell. For instance, 1.227 was selected as the optimal value for variable α after Part 1, and could be seen right below the color-filled cell in Part 1. This value remained constant during the remainder of the parametric studies. Another way to understand the table is to use the diagonally-arranged color-filled cells to divide the table into two zones. The upper zone represents the initial values of the variables that had not yet been subject to changes during the studies, while the lower zone represents the optimal values of the variables. As shown in Table 1, the optimal values for α, T, β, and i are 1.227, 4, 0.85, and 550, respectively.

Based on the initial values of the four variables, the average computational time was around 2 min, and the maximum computational time could reach almost 4 and a half minutes. The optimal values obtained through parametric studies improved the performance of the back-calculator by reducing the average computational time to 20 s and the maximum computational time to less than 1 min, which was considered to be short, and very reasonable for achieving the objectives associated with the standalone back-calculator. The resultant support conditions generated from the twenty randomized initial conditions also turned out to be identical, indicating that the optimization algorithm was robust in approximating the global optimum. When incorporated into Railroad Infrastructure 4.0, the four variables may need to be further tuned, depending on the end-users' demand on the efficiency of the ballast support condition assessment system.

Previous attempts were made to investigate the efficiency and consistency of the support condition back-calculator with a larger number of bins. However, for a single set of input moments and rail seat loads, the resultant support conditions were different when computed from different initial conditions. The limited number of input variables and boundary conditions is the likely cause for the inconsistency in results when attempting to increase resolution. Therefore, the ballast support condition was evenly divided into six discrete bins along the sleeper, and the same number of bins were later used in laboratory validation as well as field measurement. However, given that laser and optical fiber have the potential to be developed to measure more strains at a shorter distance, the number of bins can become larger and thus more realistic ballast support conditions can be computed.

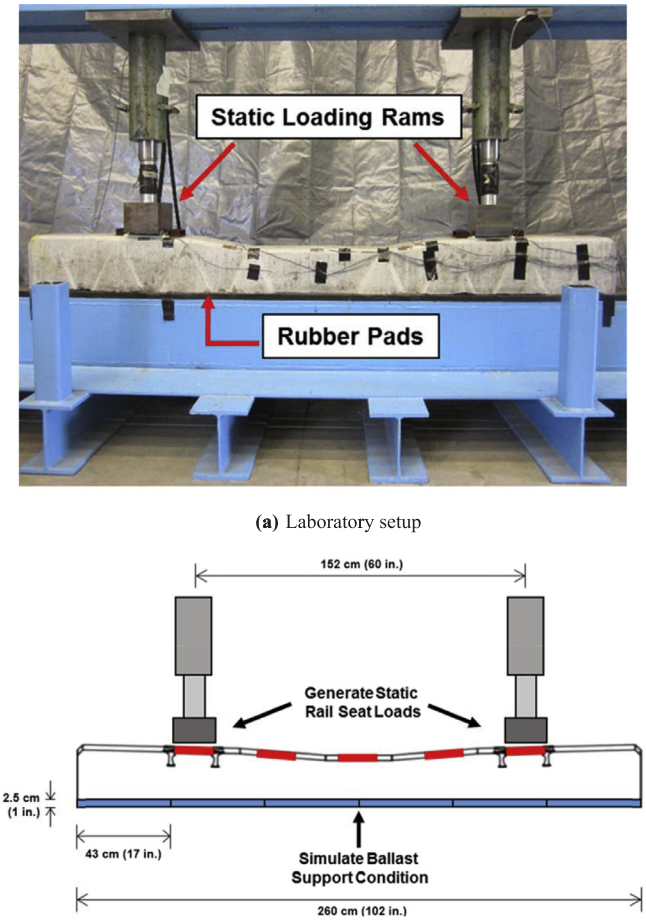

(a) Laboratory setup

(b) schematic profile view drawing

Fig. 7. Static Load Testing Machine (SLTM) at UIUC: (a) Laboratory setup; and (b) Schematic profile view drawing.

Laboratory validation

The parametric studies explained in the previous section ensured the efficiency and consistency of the ballast support condition assessment system, but to validate the accuracy of the results calculated within the Cloud Computing element and Railroad Infrastructure 4.0 as a whole, laboratory experiments were conducted at the Research and Innovation Laboratory (RAIL) at UIUC. A 260 cm (102 in.) long concrete sleeper that had previously been in service in a North American heavy haul freight track was selected for the experimentation. No visible vertical cracks were observed on the sleeper. Five surface strain gauges were mounted on the sleeper following the same orientation and locations as mentioned above, and were calibrated to provide a means to convert strains to bending moments through iterations of calibration testing.

The Static Loading Testing Machine (SLTM) at UIUC was used for this phase of laboratory experimentation. As can be seen in Fig. 7, the SLTM has two loading rams, one at each rail seat. Hydraulic hand pumps were used to manually pressurize the rams to generate static rail seat loads. The loading face of the rams had a smooth surface with a 15 cm (6 in.) width to simulate a rail base and to establish the static loads could be uniformly distributed across the entire rail seats, ensuring that the uniformly distributed rail seat load assumption made in

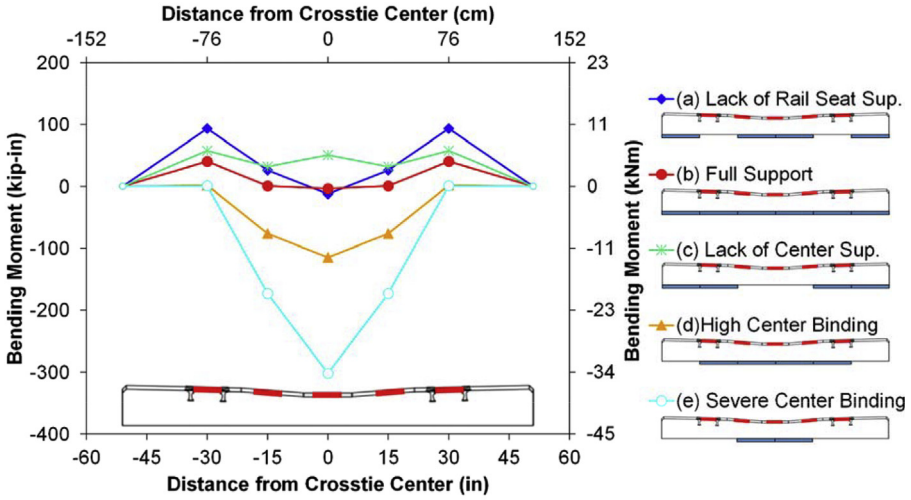

Fig. 8. Laboratory support conditions and corresponding moment diagrams.

the ballast support condition assessment system was also achieved in the laboratory experimentation. Beneath the instrumented sleeper was a series of rubber pads. Given the stiffness of the rubber pads was found to be comparable to the stiffness of the track substructure typically seen in the field, the rubber pads were used to simulate ballast support [3]. To replicate the composition of six discrete bins in the support condition back-calculator, the width of the rubber pads was designed to be identical to the bin width (43 cm (17 in.)).

Several experiments were conducted on the instrumented sleeper with varying support conditions. By rearranging the rubber pads, a total of five support conditions were created for the experiments

(Fig. 8). Each of the support conditions represents a ballast distribution commonly seen in the field [3]. For each support condition, the sleeper was loaded from 0 to 44.5 kN (10 kips) at both rail seats and the strain data were recorded while the rail seat loads were kept at 44.5 kN (10 kips). Bending moments could later be converted from the strain data at five discrete locations along the sleeper. Combined with zero moments at the two ends of the sleeper, seven bending moments constituted the moment diagram for each support condition, as shown in Fig. 8. No crack was observed on the sleeper during the loading process.

The seven bending moments and two static rail seat loads were used as inputs for the standalone support condition back-calculator to back-calculate the reaction force distribution. The comparisons between the laboratory setups and back-calculator results can be seen in Fig. 9. The vertical red[1] lines shown in the back-calculator results represent the reaction force exerted at the bottom of the sleeper. The longer the red lines, the greater the reaction force. The calculated reaction force distributions were comparable to the physical arrangements of the rubber pads, that is, the majority of the reaction forces were distributed at bins where the rubber pads were laid. One seemingly "inconsistent" comparison was between the full support condition (Fig. 9(a)), where the back-calculator result shows that the reaction forces were more concentrated below the rail seat sections rather than being uniformly distributed along the sleeper. However, the full support condition only implied that the bottom of the sleeper was in full contact with the support layer, and it was not guaranteed that the pressure along the bottom of the sleeper would remain constant. In fact, when loaded, the center portion of the sleeper curled upwards while the rail seat sections translated downwards. This bending behavior caused the reaction forces to be more concentrated below rail seat sections, as illustrated by the back-calculator. Therefore, for the laboratory experiments conducted for each rubber pad arrangement, the support condition back-calculator generated a reasonable result. Even though the resultant reaction distributions were not sensitive enough to capture the change of reaction forces within each bin, given the limited number of input variables, the authors were comfortable with the accuracy of the ballast support condition assessment system for visualizing and quantifying the general support condition a concrete sleeper might experience.

Field experimentation and monitoring results

Field experimentation

After validation with extensive laboratory experiments, the automatic ballast support condition assessment system was deployed at a tangent location on a Class I heavy axle load (HAL) freight railroad in the western United States to examine its performance and monitor the support conditions over time. The field site was located in Nebraska (NE) and was subjected to approximately 200 million gross tonnes (MGT) of freight traffic in 2014. One of the benefits of selecting this particular location was the consistency of train loading; almost all of the traffic on this line was unit-coal trains with similar locomotives and cars, which resulted in little variance in wheel and axle loads. Further, Wheel Impact Load Detectors (WILD), which can provide actual wheel load values which can then be converted into rail seat input loads, were installed nearby. A schematic of the field experimentation map and a photo after installation are shown in Fig. 10.

As shown in Fig. 10(a), the test site had two zones, spaced approximately 18 m (60 ft) apart, with each zone consisting of five sleepers. Based on visual inspection only, Zone 1 was selected as a poorly supported zone because, upon train passes, this zone was observed to deflect more than Zone 2 [33]. Two thermocouples were installed on a sleeper between the two zones, one at the sleeper top chamfer and one near the sleeper bottom covered in ballast. These were deployed to measure the temperature gradient between the top and bottom of the sleeper [33,5]. The wheel load data provided by the nearby WILD were used to calculate the rail seat loads experienced by the sleepers. Since the wheels passing through the test site regularly had a nominal wheel load of 160 kN (36 kips) (Fig. 11), the rail seat load could be approximated to be 80 kN (18 kips) according to AREMA MRE Figure 30-4-1 [1], and this value was used as the input rail seat load for the support condition assessment. The concrete sleeper at the site was 260 cm (102 in.) long and was waisted (tapered) at the center. The ballast layer is constructed with granite aggregate with a grain size

[1] For interpretation of color in Figs. 9, 15 and 16, the reader is referred to the web version of this article.

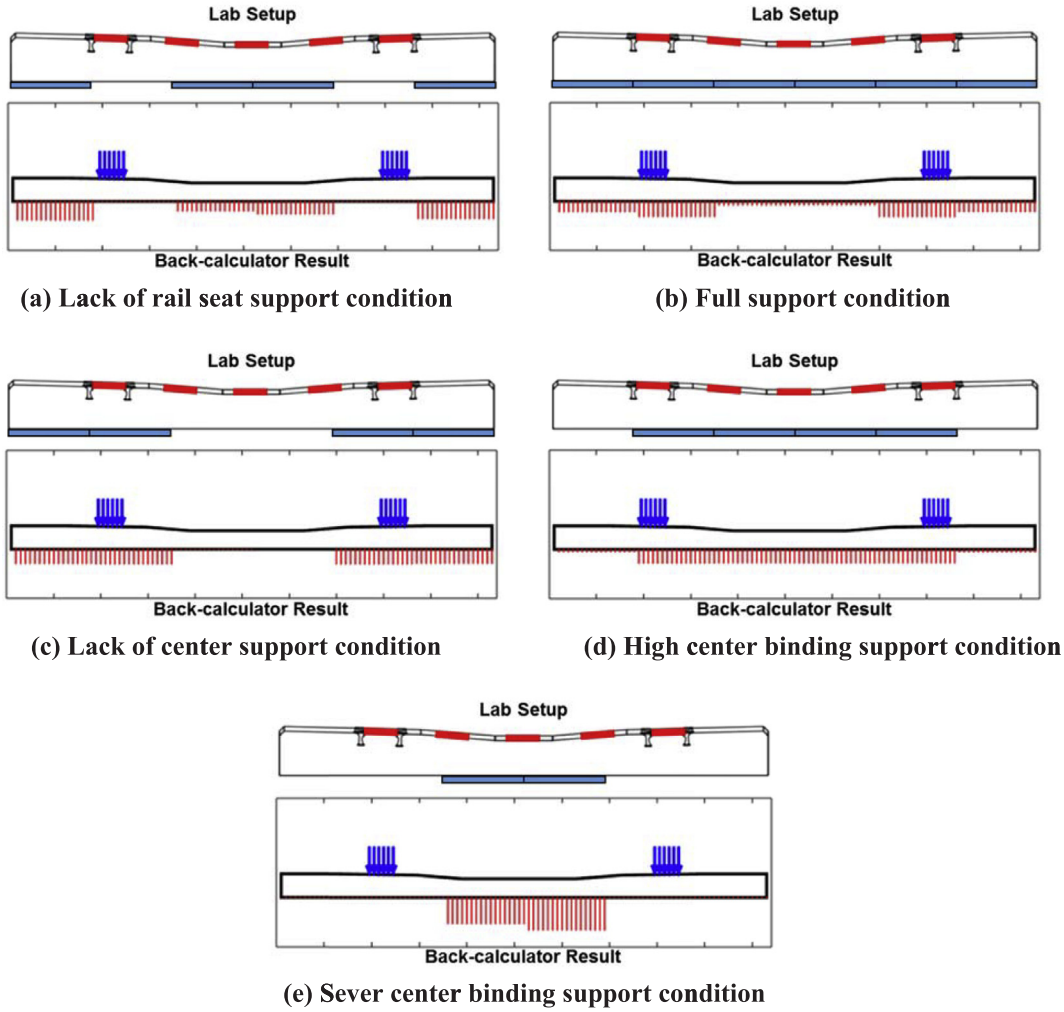

Fig. 9. Comparisons between laboratory setup and back-calculator results under five unique support conditions.

distribution that met the AREMA No. 4 gradation requirements [1]. The sleepers, which have a 1:30 cant at the rail seat, were installed in 1999 and spaced at 610 mm (24 in.) on center.

Developed ballast support assessment system calculation procedures

Introduced in Section 2, a back-calculator was developed as part of the automatic ballast support condition assessment system to compute ballast pressure distribution subjected to revenue service loading in real-time. Fig. 12 illustrates the work flow for the developed automatic ballast support condition assessment system.

Existing ballast pressure limit states

Ballast pressure distributions were used to represent the various sleepers' support conditions. Under an assumption of uniform support, the ballast pressure can be calculated as 221 kPa (32 psi). There are two ballast pressure limit states defined by the AREMA MRE [1] to aid the evaluation of the ballast condition.

1. AREMA MRE indicates that the allowable ballast pressure under concrete sleepers to be 586 kPa (85 psi) to control ballast crushing.
2. AREMA MRE recommends an allowable subgrade bearing stress of 172 kPa (25 psi) to control subgrade permanent deformation, which could be calculated using the Talbot equation (Eq. (9)).

$$h = \left(\frac{16.8p_a}{p_c}\right)^{\frac{4}{5}} \tag{9}$$

where, h = support ballast depth

p_a = pressure at sleeper-ballast interface
p_c = pressure at subballast-subgrade interface.

Since the test site was considered to be well-maintained, the total depth of ballast and subballast was assumed to be 46 cm (18 in.) according to AREMA, and the ballast pressure (p_a) was then calculated to be 379 kPa (55 psi) from Eq. (9).

Ballast pressure index

To better analyze the variation of ballast pressure beneath the sleepers, the Ballast Pressure Index (BPI) was developed. BPI is a quantifiable value that can aid in quantifying the uniformity of ballast pressure distribution. BPI is defined as the ballast pressure computed from the ballast support condition assessment system, normalized to the theoretical uniform ballast pressure within each bin of the sleeper model, as shown in Eq. (10).

$$BPI = \frac{P_{comp}}{P_{uni}} \tag{10}$$

where, BPI = Ballast Pressure Index

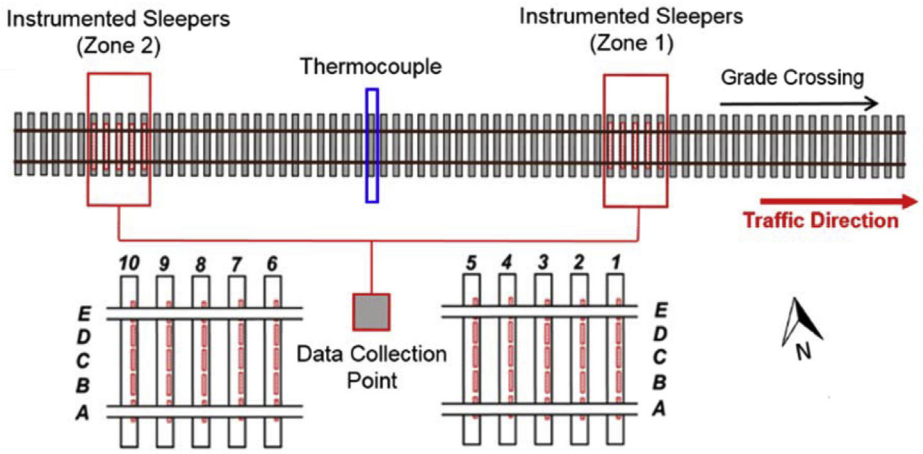

(a) Schematic map

(b) Photo during and after installation

Fig. 10. Field instrumentation site: (a) Schematic map; (b) Photo during and after installation.

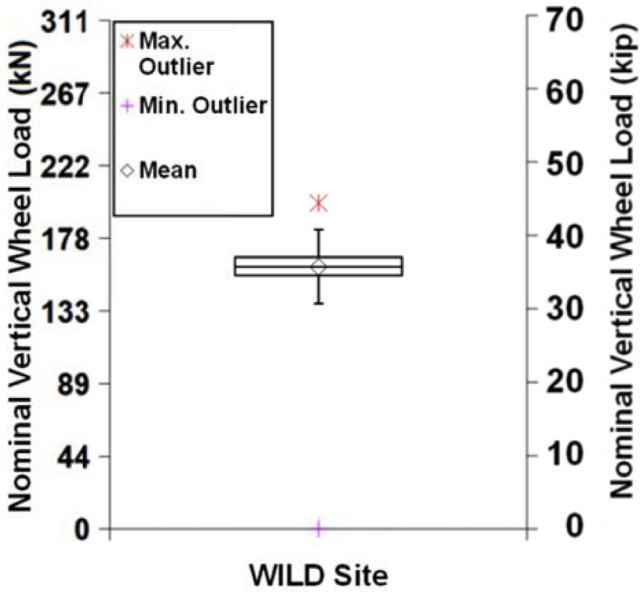

Fig. 11. Wheel loads provided from nearby WILD site for 74 trains over 9 visits spanning March through September 2015.

P_{comp} = pressure computed
P_{uni} = pressure based on the assumed uniform support.

For a certain sleeper bin, if the ballast support satisfies the uniform support assumption, then the computed ballast pressure will be the same as the uniform ballast pressure, making the BPI equal 1. When a void develops in a sleeper bin, the computed ballast pressure becomes 0, so does the BPI for that particular bin. A sleeper bin is considered to be a hotspot if the computed ballast pressure exceeds the AREMA allowable ballast surface stress, because the exceedance indicates the potential for accelerated ballast deterioration, which poses a threat to safe railroad operations. Therefore, for this particular test site, the BPI value of a hotspot is calculated to be 2.66 (586 kPa divided by 221 kPa). Note the uniform support condition, BPI = 1, is not necessarily the optimal support condition. The BPI is to provide the ratio of the actual ballast pressure to the calculated ballast pressure in uniform support condition. The acceptable or optimal BPI should be determined based on the allowable subgrade and ballast bearing pressure of the specific track section.

Example calculation of one field measurement

To demonstrate how raw measurements collected at the field site were computed and translated into valuable ballast information, a set of data from one sleeper under one series of wheel passes is used as an example. Once the wheel passed over the sleeper, the bending of the sleeper caused the strain gauges to elongate, changing the electrical resistance of the gauges. The voltages associated with each of the strain

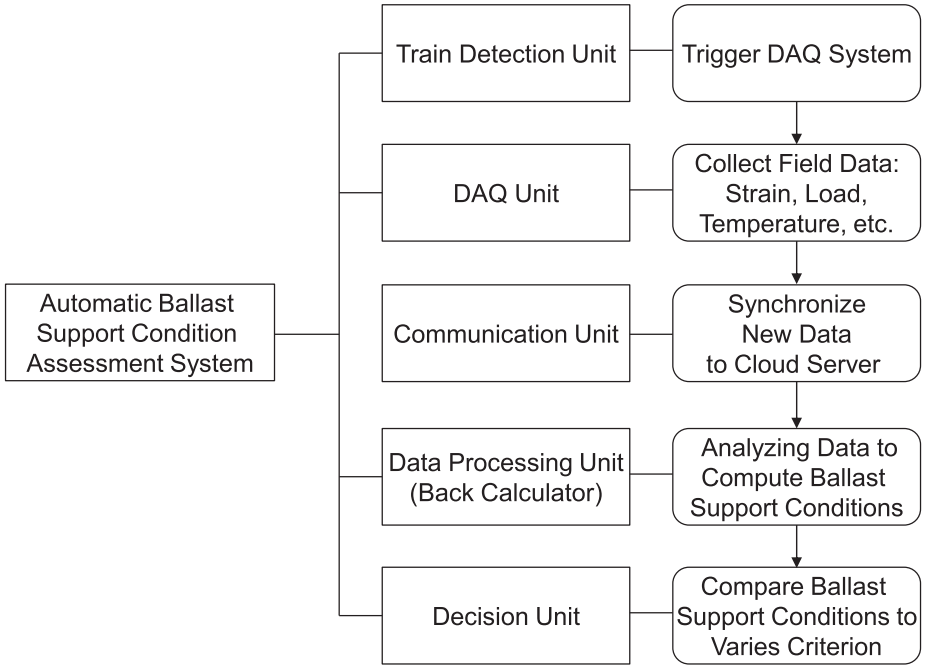

Fig. 12. Component and work flow of the ballast assessment system.

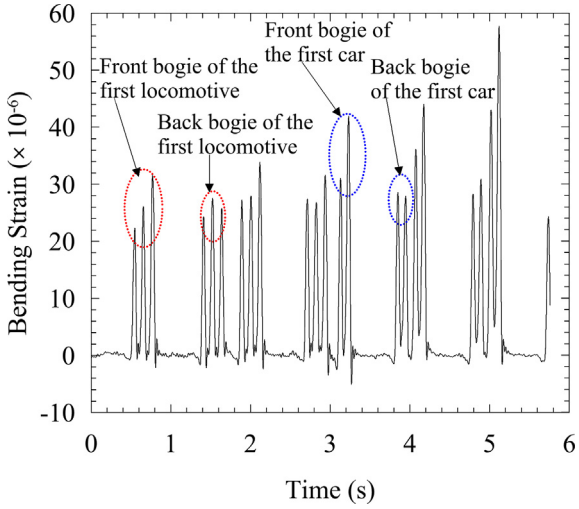

Fig. 13. Sample strain gauge data.

gauges was therefore affected. Fig. 13 gives an example of the strain gauge readings under 23 consecutive wheel loads. The sampling rate was 2000 Hertz for this study.

Through the multiplication of a pre-programmed factor provided by the strain gauge manufacturer, the change in voltage could be converted into micro-strain [33]. In this particular sample set, the five strain gauges measured −46.05, 156.17, 206.08, 75.24, and −63.57 micro-strains, respectively. Before the on-site installation, the sleepers of the same model and similar year had been calibrated in the lab so that each strain measurement could be converted into bending moment [8]. In this case, the calibration factors for the rail seat gauge was −0.0894 kN m/με (−0.7909 kip-in/με), and the calibration factors for the intermediate gauge and center gauge were −0.0782 kN m/με (−0.6917 kip-in/με) and −0.0669 kN m/με (−0.51 kip-in/με), respectively [33]. The bending moment profile could then be developed by multiplying the strain data with the corresponding calibration factors. From one rail seat to another, the bending moments were 4.11 kN m (36.42 kip-in), −12.20 kN m (−108.02 kip-in), −13.78 kN m (−121.98 kip-in), −5.88 kN m (−52.04 kip-in), and 5.68 kN m (50.28 kip-in) based on the measured strain.

After the bending moment profile was developed, the next step was to input those moment values, along with the rail seat load, into the ballast condition back-calculator and generate the reaction profile of the sleeper. After iterations of calculation and optimization mentioned earlier (refer to Section 2), the percentage of reaction within each bin was computed. Fig. 14 presents the initial, final, and the intermediate results during the iterations of the back-calculator processing. Note that the back-calculator started with uniform support regardless of the initial bending moment. The round markers in the moment graphs in Fig. 14 are the measured bending moments. Once the calculated bending moment values match the measured values within the tolerance (Fig. 14(f)), the calculation is completed (refer to Section 2 for details).

The final results of the percentage of support from Bin 1 to Bin 6 in this example were 14.3%, 5.1%, 35.5%, 16.3%, 19.2%, and 9.6%, which was obtained after 550 iteration steps within 60 s of computation time. The percentage of each bin represents the relative support provided by the bin. Multiplying the percentage by the total magnitude of the applied load and dividing by the length and width of each bin, the ballast pressures were then calculated for all six bins and they were 190.3 kPa (27.6 psi), 67.6 kPa (9.8 psi), 544.7 kPa (79.0 psi), 250.3 kPa (36.3 psi), 255.1 kPa (37.0 psi), and 126.9 kPa (18.4 psi), respectively. Finally, the BPI values could be computed by dividing the pressure by the theoretical uniform ballast pressure (220 kPa (32 psi) in this case), and they were 0.86, 0.31, 2.47, 1.13, 1.16, and 0.58, respectively. Again, a BPI close to 1 indicates uniform support, less than 1 indicates the development of a void, and higher than 1 indicates higher stress concentration on the ballast surface than uniform support.

Ballast support assessment for multiple sleepers under one axle pass

The previous section introduced the calculation process for calculating the ballast pressure distribution under a single sleeper. Fig. 15 shows the resultant ballast pressure distribution when several instrumented sleepers were subjected to the same axle from a train pass at around 8:00 a.m. on 26 May 2015. The ballast pressure limit states are depicted in Fig. 15 as three horizontal dashed lines. To better display

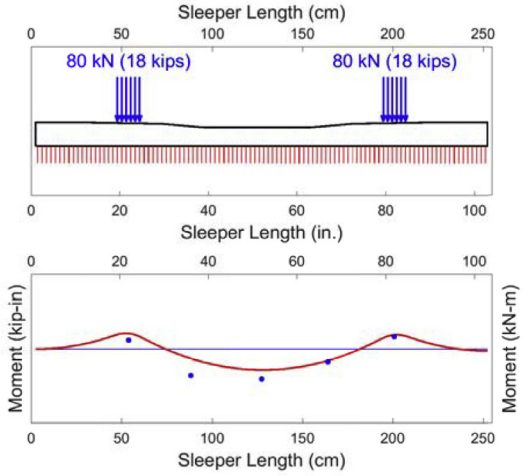

(a) Initial condition, iteration step 0

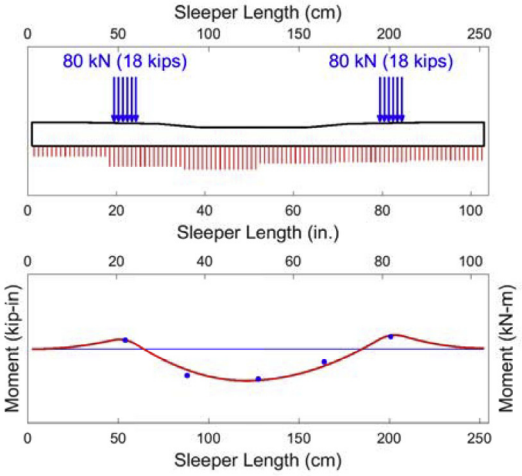

(b) Intermediate result, iteration step 100

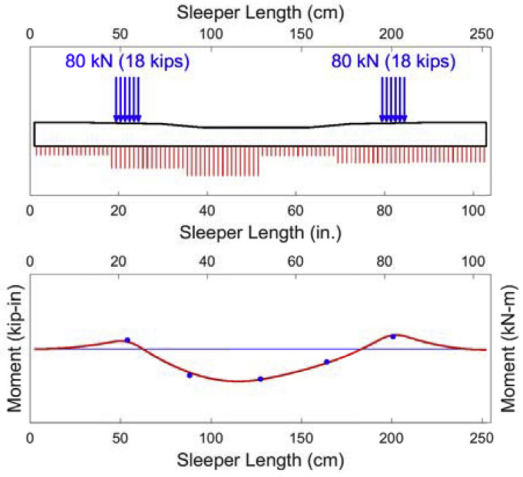

(c) Intermediate result, iteration step 200

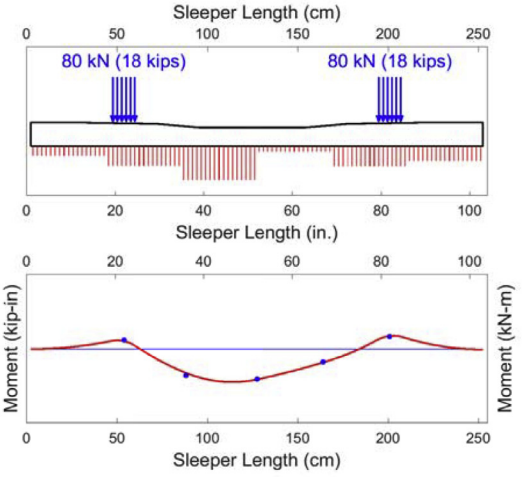

(d) Intermediate result, iteration step 300

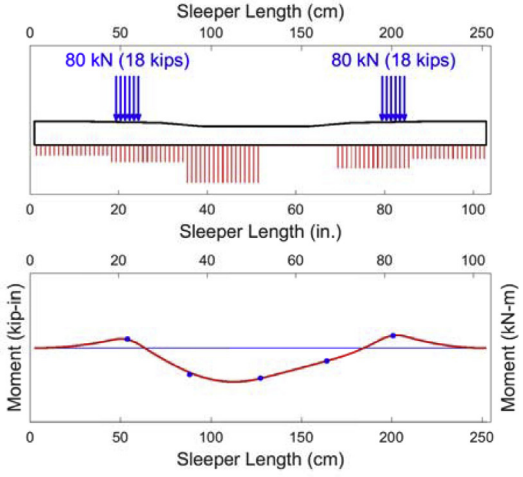

(e) Intermediate result, iteration step 400

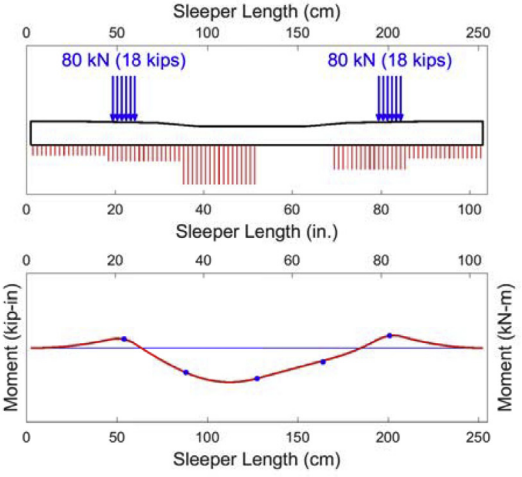

(f) Final result, iteration step 550

Fig. 14. Sample ballast support condition calculation at different iterations.

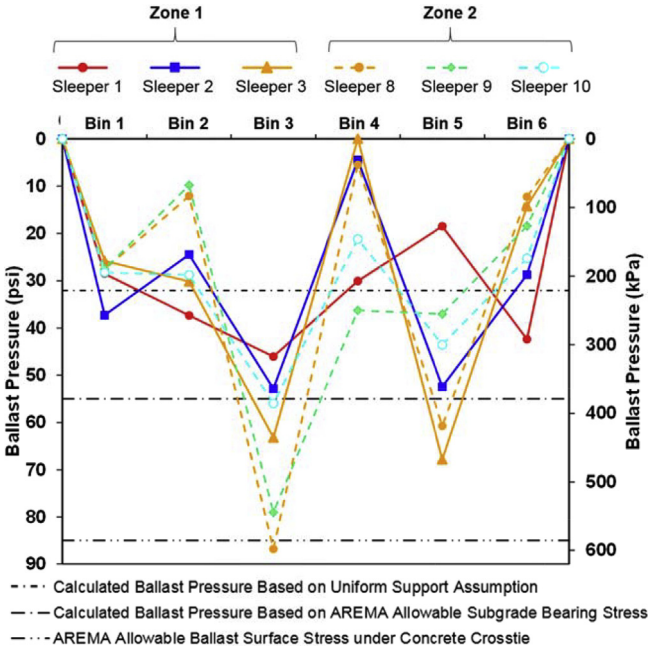

Fig. 15. Ballast pressure distributions for six sleepers under one loaded axle.

the results, the uniformly distributed pressure within each bin was simplified into a single point located at the centerline of each bin and having the same magnitude as the uniform pressure. The points within the six bins were connected together by straight lines to form the pressure distribution profile. To clearly depict the results in a single graph, only three out of five sleepers were selected from each zone. Variation of ballast support conditions can be seen among the adjacent sleepers. As shown in Fig. 15, ballast pressures varied for all sleepers in both zones, but Zone 1 experienced a slightly higher variation, where the mean percent difference among ballast pressure distributions in Zone 1 was 55%, 8% greater than the mean percent difference in Zone 2. It is noticeable that the pressure in Bin 4 of Sleeper 3 was almost zero, which means that within Bin 4 of Sleeper 3, a void had developed at the sleeper-ballast interface. In addition, the ballast pressures of some sleepers exceeded the ballast pressure limit computed based on the allowable subgrade bearing stress. This indicates that subgrade bearing capacity failure could occur if this exceedance continued to happen. However, based on the maintenance record of the railroad, the subgrade quality at this location exceeds the requirement by the AREMA MRE [1]. Thus, the actual ballast pressure that would induce an excessive subgrade pressure could be higher than the current value, meaning that it is likely that this site would not experience a subgrade bearing capacity failure. The allowable ballast surface stress was also exceeded on a few occasions within Bin 3 of Sleeper 8. If this exceedance persisted, accelerated ballast deterioration could be expected.

Fig. 16 shows the color-coded BPI distribution for all ten instrumented sleepers under the same loaded axle used in Fig. 15. Green represents the uniform support scenario, where the BPI value is 1; blue represents voids, where the BPI value is 0; red represents hotspots, where the BPI value is not less than 2.66. The more consistent green there is for a sleeper shown in Fig. 16, the more uniform the ballast support was beneath that sleeper. Following this logic, among all ten instrumented sleepers, Sleeper 1 and 10 had the most uniform support conditions. Besides demonstrating the uniformity of the ballast support condition, this color-coded BPI distribution can also pinpoint the voids and hotspots within the system. As can be seen in Fig. 16, hotspots were solely developed within Zone 2, and next to each hotspot bin were two adjacent bins showing bluish colors, suggesting that voids might develop somewhere within those bins. This significant BPI difference among the adjacent bins implies that those sleepers in Zone 2 were not as properly supported as those in Zone 1. The evaluation contradicts the visual inspection conducted at the beginning of the field installation, which considered Zone 1 as poorly supported. The contradiction not only indicates that visual inspection could be misleading, but also justifies the analysis of the ballast support condition at the sleeper-ballast interface.

Ballast pressure variation over one day

Concrete sleeper curling behavior under temperature gradient was well documented by Wolf et al. [33]. When the top of the sleeper is exposed to sunlight, it experiences higher temperature as opposed to the sleeper bottom that is buried in the ballast. This difference in temperature, or the temperature gradient, causes the top of the sleeper to elongate more, inducing the sleeper to curl upwards at the sleeper center [33]. Due to the upward curling behavior, the center section of the sleeper will have less contact with the ballast, while the rail seat section or the end of the sleeper will have more contact with the ballast. In order to quantify this redistribution of ballast support, data from two train passes were captured on the same date, one around 1:00 A.M., and

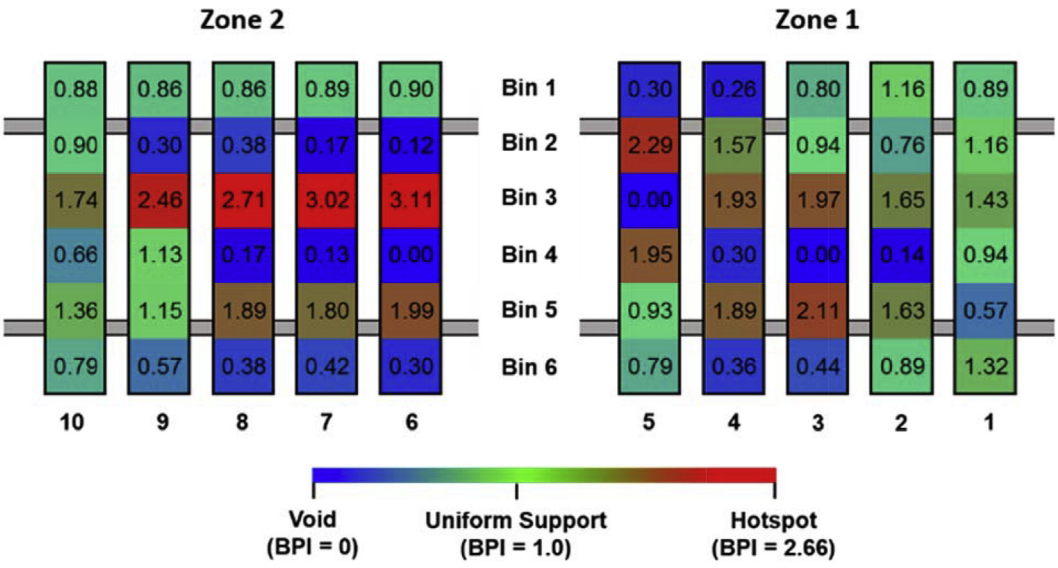

Fig. 16. BPI distribution for ten sleepers under one loaded axle.

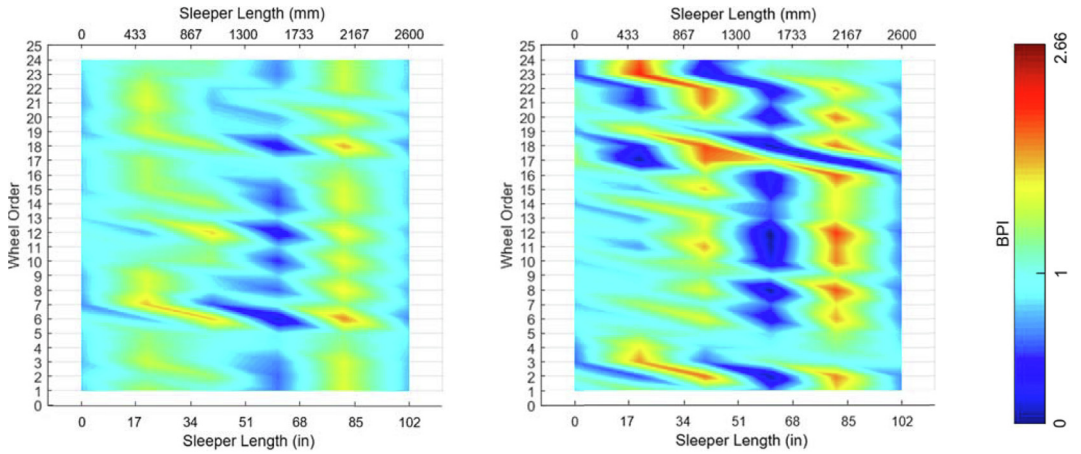

(a) Train Pass at 1 A.M. (b) Train Pass at 7 A.M.

Fig. 17. BPI distribution for one sleeper with 3°F temperature gradient increase.

the other one around 7:00 A.M. During the time period, thermocouples were continuously collecting data, and the temperature gradient was measured and found to be consistently increasing.

Fig. 17 shows the BPI distributions under a loaded axle for each of the train passes on that date. The x-axis shows the length of the sleeper in question, and the y-axis shows the number of wheels passing over the sleeper. To simplify the results and provide greater clarity, results from only 24-wheel passes are included. The color shown on the distribution indicates the BPI value at each coordinate; similar to Fig. 16. Blue indicates a BPI value of 0, green represents a BPI value of 1, and red represents a BPI value of 2.66 or above. As temperature gradient increased, the BPI values in the center section of the sleeper (Bin 3 and Bin 4) decreased. At the same time, the rail seat sections of the sleeper (Bin 2 and Bin 5) showed an increase in BPI, indicating that the temperature gradient effect was so prevailing on the curling behavior of the sleeper that voids were created at the center section of the sleeper and hotspots were created at the rail seat regions.

Ballast pressure variations between months

In order to investigate the variation of ballast support conditions as a function of time or tonnage accumulation, two more site visits were made on 8 July 2015 and 14 August 2015, and data were collected for a train pass at around 8:00 a.m. during both site visits. Fig. 18 shows the BPI distributions from all three site visits. Similar to Fig. 16, for each date, the BPI distribution was based on a single loaded axle of the 8:00 a.m. train pass. To clearly demonstrate all three BPI distributions on a single figure, each sleeper bin was cut into three sections from the bottom-left corner, with the top-left section representing the BPI value from 26 May 2015, the middle section the BPI value from 8 July 2015, and the bottom-right section the BPI value from 14 August 2015. By doing so, the change in BPI value can be observed clockwise within each sleeper bin.

As illustrated in Fig. 18, throughout the 4-month period and approximately 31.8 million gross tonnes (mgt) (35 million gross tons (MGT)) of accumulated tonnage, the BPI distribution for all ten sleepers remained generally constant. Among three site visits, the maximum BPI increase was 0.74 (or 163 kPa (23.6 psi) in ballast pressure), whereas the maximum BPI decrease was 0.80 (or 176 kPa (25.6 psi) in ballast pressure).

One would expect that as tonnage increased, the ballast support condition would become more center-bound. However, this change in ballast support condition could not be easily observed in the test site. On the contrary, based on the BPI distributions, Zone 2 showed the opposite ballast behavior. Hotspots were predominant in Sleepers 6, 7, and 8 during the first site visit, but after four months, the BPI values for those hotspots decreased by a mean of 18%, and they were no longer above the hotspot limit of 2.66; this could indicate that the ballast had deteriorated or moved to allow for improved stress distribution. Factors other than tonnage accumulation might have more impact on this change of ballast support condition, such as change in ballast moisture content, change in ballast particle shape, and change in temperature.

Conclusions

Railroad Infrastructure 4.0, adopted from the concept of Industry 4.0, is proposed as a revolutionary system for railroad track maintenance prioritization and management. The four elements - Sensor Monitoring, Cloud Computing, Decision Making, and Problem Solving - ensure that Railroad Infrastructure 4.0 is an automated, effective, cost-efficient, and self-learning system capable of integrating new techniques. To serve as an example, the ballast support condition assessment system was introduced. The ballast support condition assessment system was developed as a computer-aided tool to quantify the ballast condition at the sleeper-ballast interface. From this work, several conclusions were drawn from the development and application of this system.

- The optimization algorithm, consisting of bi-polar Pareto Distribution and simulated annealing, ensured that the computational time was acceptable for this application (i.e. analysis took no longer than 1 min for the chosen result resolution).
- For a certain set of input variables, the back-calculator results were identical regardless of how different the initial random support condition was generated to be at the start of computation (i.e. the back-calculator was considered to be a robust tool that accurately quantified the support condition).
- During laboratory validation, the support conditions calculated from the back-calculator were representative of the actual support conditions.
- Ballast pressure varied within each instrumented sleeper, as well as among adjacent sleepers. The difference of ballast pressure at different sections of the same sleeper can be as much as a factor of six.
- Color-coded BPI distribution provided an effective method to not only evaluate the uniformity of ballast distribution, but also to identify voids and hotpots at the sleeper-ballast interface.
- Based on data from three site visits, the accumulation of tonnage did not have a significant impact on the ballast pressure distribution, partially because the test site had been well-maintained.
- The developed automatic ballast support condition assessment system can assist the rail industry in optimizing ballast surfacing cycles, enhancing safety, and reducing operating cost.

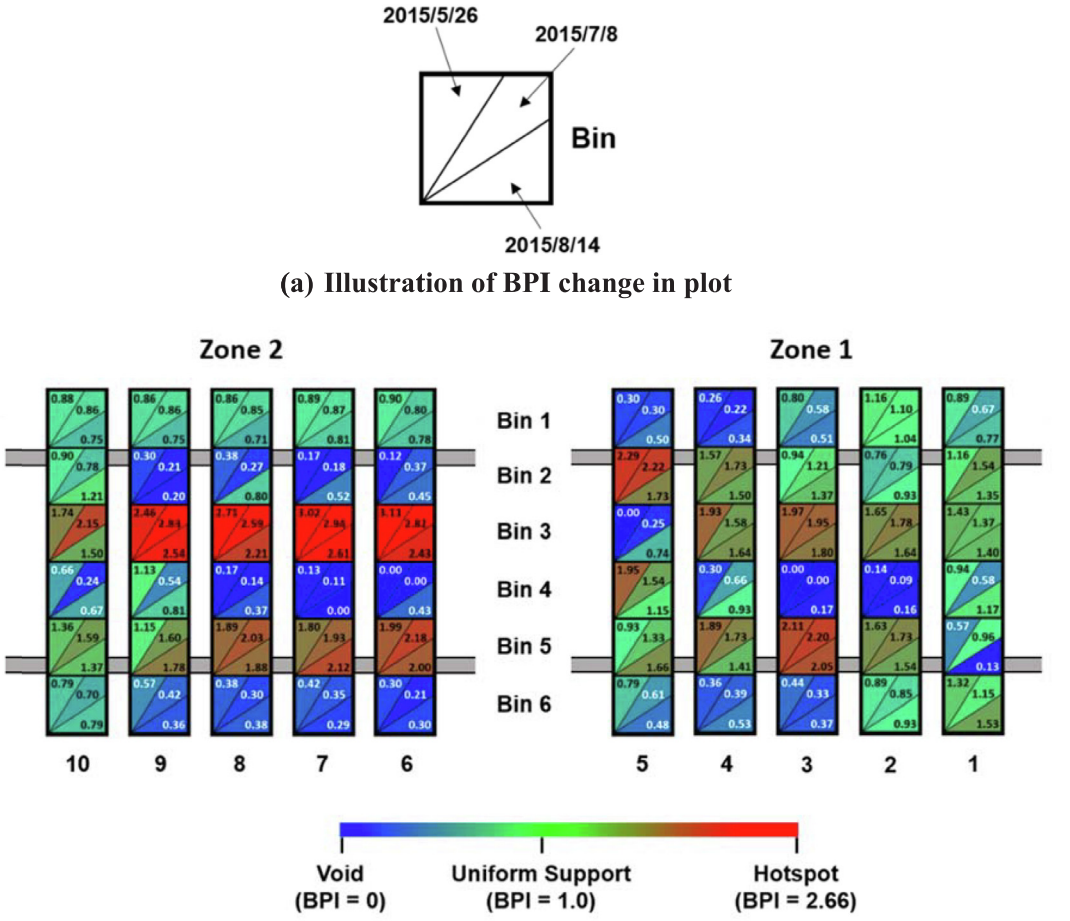

Fig. 18. BPI distributions for three site visits on 26 May, 8 July, and 14 August 2015.

Acknowledgements

Portions of this research effort were funded by the Federal Railroad Administration (FRA) and Federal Transit Administration (FTA), within the United States Department of Transportation (USDOT). The material in this paper represents the position of the authors and not necessarily that of FRA or FTA. The authors are grateful for the guidance and valuable feedback provided by Henry Wolf and Prof. Ouyang Yanfeng from UIUC during the development of the back-calculator. The authors would also like to thank Josue Bastos, Alejandro Alvarez, Brevel Holder, Camila Silva, and Matheus Trizotto for their assistance with laboratory experimentation, as well as Matt Csenge, Phanuwat Kaewpanya, and Quinn Todzo for their assistance with data processing. J. Riley Edwards has been supported in part by grants to the UIUC Rail Transportation and Engineering Center (RailTEC) from CN and Hanson Professional Services, Inc.

References

[1] American Railway Engineering and Maintenance-of-Way Association (AREMA). Manual for Railway Engineering. Lancaster, MD; 2016.
[2] Association of American Railroads (AAR). Total annual spending 2013 data. Annual report; 2013.
[3] Bastos JC. Analysis of the performance and failure of railroad concrete sleepers with various track support conditions. Urbana, Illinois: University of Illinois at Urbana-Champaign; 2016. M.S. Thesis.
[4] Butter CD, Hocker GB. Fiber optics strain gauge. Appl Opt 1978;17(18):2867–9.
[5] Canga Ruiz AE, Qian Y, Edwards JR, Dersch MS. Analysis of the temperature effect on concrete crosstie flexural behavior. Constr Build Mater 2019;196:362–74.
[6] Čebašek TM, Esen AF, Esen AF, Woodward PK, Laghrouche O, Connolly DP. Full scale laboratory testing of ballast and concrete slab tracks under phased cyclic loading. Transp Geotech 2018;17A:33–40.
[7] Connor P, Schmid F. Train protection; n.d. Retrieved from < http://www.railway-technical.com/signalling/train-protection.html > .
[8] Edwards JR, Gao Z, Henry WE, Dersch MS, Qian Y. Quantification of concrete railway sleeper bending moments using surface strain gauges. Measurement 2017;111:197–207.
[9] Edwards JR, Canga Ruiz AE, Cook AA, Dersch MS, Qian Y. Quantifying bending moments in rail transit concrete sleepers. ASCE J Transport Eng, Part A: Syst 2018;144(3):04018003.
[10] Englander JA, Englander AC. Tuning monotonic basin hopping: improving the efficiency of stochastic search as applied to low-thrust trajectory. Proceedings of international symposium on space flight dynamics, Laurel, MD, May 5–9. 2014.
[11] Hermann M, Pentek T, Otto B. Design Principles for Industrie 4.0 Scenarios. In: 49th Hawaii international conference on system sciences (HICSS), January 5–8, Koloa, HI, USA; 2016.
[12] Hibbeler RC. Engineering mech.: statics. 14th ed. London, United Kingdom: Pearson; 2015.
[13] Kashani HF, Hyslip JP, Carlton HL. Laboratory evaluation of railroad ballast behavior under heavy axle load and high traffic conditions. Transp Geotech 2017;11:69–81.
[14] Kirkpatrick S, Gelatt CD, Vecchi MP. Optimization by simulated annealing. Sci, New Ser 1983;220(4598):671–80.
[15] Laarhoven PJ, Aarts EH. Simulated annealing: theory and applications. Houten, Netherlands: Springer; 1987.
[16] L.B. Foster Salient Systems. Wheel Impact Load Detector (WILD); n.d. Retrieved from < http://www.lbfoster-salientsystems.com/Wheel_Impact_Load_Detector.asp > .
[17] Le Pen L, Powrie W, Zervos A, Ahmed S, Aingaran S. Dependence of shape on particle size for a crushed rock railway ballast. Granular Matter 2013;15(6):849–61.
[18] Liu S, Huang H, Qiu T. Laboratory development and testing of "smartrock" for railroad ballast using discrete element modeling. In: Proceedings of 2015 joint rail conference. San Jose, California, USA, March 23–26; 2015.
[19] MATLAB and signal processing toolbox 2013b. The MathWorks, Inc., Natick, MA.

[20] McGonigal RE. Ballast: to keep 'em rolling, it takes plenty of rock." Trains: the magazine of railroading, May 1; 2006.
[21] McHenry MT. Pressure measurement at the ballast-tie interface of railroad track using matrix based tactile surface sensors. Lexington, Kentucky: University of Kentucky; 2013. M.S. Thesis.
[22] Monserrat O, Crosetto M. Deformation measurement using terrestrial laser scanning data and least squares 3D surface matching. ISPRS J Photogramm Remote Sens 2008;63(1):142–54.
[23] Ngo NT, Indraratna B, Rujikiatkamjorn C. Micromechanics-based investigation of fouled ballast using large-scale triaxial tests and discrete element modeling. J Geotech Geoenviron Eng 2017;143(2):[04016089]. https://doi.org/10.1061/(ASCE)GT.1943-5606.0001587.
[24] Selig ET, Waters JM. Track geotechnology and substructure management. London, England: Thomas Telford Ltd.; 1994.
[25] SmartRail World. Launch of world's longest driverless freight railway is delayed in Australia. April 25; 2016. Retrieved from < https://www.smartrailworld.com/worlds-longest-driverless-freight-railway-runs-into-problems-in-australia > .
[26] Solomon B. Railway maintenance equipment: the men and machines that keep the railroads running. Minneapolis, MN: MBI Publishing Company LLC; 2001.
[27] Sun Q, Indraratna B, Ngo NT. Effect of increase in load and frequency on the resiliency of railway ballast. Géotechnique 2018. https://doi.org/10.1680/jgeot.17.p.302.
[28] The Railway Technical Website. Automatic Train Control; n.d. Retrieved from < http://www.railway-technical.com/signalling/automatic-train-control.html > .
[29] Thompson HB, Carr G. Ground penetrating radar evaluation and implementation. United States Department of Transportation (USDOT) Federal Railroad Administration (FRA), Research Results, July 14–24; 2014.
[30] Tracy P. Case study: Amazon embraces shipping automation, robotics; July 8, 2016. Retrieved from < https://www.rcrwireless.com/20160708/internet-of-things/amazon-automation-tag31-tag39 > .
[31] Wolf HE, Mattson S, Edwards JR, Dersch MS, Barkan CPL. Flexural analysis of prestressed concrete monoblock crossties: comparison of current methodologies and sensitivity to support conditions. In: Proceedings of the transportation research board 94th annual meeting. Washington, D.C., January 11–15; 2015.
[32] Wolf HE. Flexural behavior of prestressed concrete monoblock crossties. Urbana, Illinois: University of Illinois at Urbana-Champaign; 2015. M.S. Thesis.
[33] Wolf HE, Qian Y, Edwards JR, Dersch MS, Lange DA. Temperature-induced curl behavior of prestressed concrete and its effect on railroad crossties. Constr Build Mater 2016;115:319–26.